



Optics Letters

Optical frequency combs generated mechanically

M. SUMETSKY

Aston Institute of Photonic Technologies, Aston University, Birmingham B4 7ET, UK (m.sumetsky@aston.ac.uk)

Received 29 May 2017; revised 13 July 2017; accepted 15 July 2017; posted 18 July 2017 (Doc. ID 296977); published 10 August 2017

An elongated bottle microresonator with nanoscale parabolic effective radius variation can possess a series of dense equally spaced optical eigenfrequencies whose separation can match the eigenfrequency of its axially symmetric acoustic mode. It is shown that this acoustic mode can parametrically excite optical modes and give rise to a highly equidistant and moderately broadband optical frequency comb with the teeth spacing independent of the input laser power and the amplitude of mechanical vibrations.

Published by The Optical Society under the terms of the [Creative Commons Attribution 4.0 License](#). Further distribution of this work must maintain attribution to the author(s) and the published article's title, journal citation, and DOI.

OCIS codes: (060.2340) Fiber optics components; (140.3945) Microcavities; (230.3990) Micro-optical devices.

<https://doi.org/10.1364/OL.42.003197>

Among a broad class of optical microresonators including Fabry–Perot, spherical, toroidal, bottle, and photonic crystal resonators, of special interest are those that can serve as high Q -factor acoustic and optical resonators simultaneously. These microresonators exhibit fascinating phenomena of opto-acoustic coupling, including the resonant Brillouin and Raman scattering, radiation pressure interactions, and optomechanical cooling. An investigation of these phenomena emerged as a research direction in physics—cavity optomechanics (see [1–9] and references therein).

Microresonators of special interest are those having optical modes which can resonantly interact with acoustic modes. In such resonators, the separation of optical eigenfrequencies is close to their natural acoustic frequency or Brillouin frequency. The matching of two optical whispering gallery mode (WGMs) eigenfrequencies with an acoustic eigenfrequency ~ 130 MHz has been reported for a spherical microresonator with a $162\ \mu\text{m}$ radius [4]. In [5], the splitting of optical WGM eigenfrequencies of two evanescently coupled $32\ \mu\text{m}$ radius toroidal microresonators has been adjusted to match the 23 MHz acoustic eigenfrequency of one of them. Resonant opto-acoustic interaction has been demonstrated for much larger calcium fluoride and silica resonators, whose radii exceeded 2.5 mm and free spectral ranges matched the Brillouin frequencies equal to ~ 18 and 11 GHz, respectively [6,7]. Generally, for microresonators with small characteristic dimensions $\sim 100\ \mu\text{m}$, the resonant

matching condition of optical WGMs frequencies and natural acoustic frequencies ~ 100 MHz is difficult to achieve because of their small dimensions and insufficient fabrication precision.

Here we note that the ultraprecise fabrication of microresonators, which are designed to enable efficient resonant interaction of optical and acoustic modes, can be realized using the surface nanoscale axial photonics platform [10,11]. For example, two coupled identical bottle microresonators having the effective radius variation (ERV) of ~ 5 nm were fabricated in [12] at the $38\ \mu\text{m}$ diameter optical fiber with a precision better than 0.2 angstrom. The splitting of optical eigenfrequencies of these resonators was ~ 0.5 GHz and could be reduced further by post-processing. In another example, a bottle resonator with a 2.8 nm ERV demonstrated in [11] had the free spectral range ~ 180 MHz. The separation of optical eigenfrequencies in both examples was comparable to the natural breathe frequencies of these resonators (see [13] and calculations below).

Recently, it has been experimentally demonstrated that the axially symmetric breathe acoustic modes of a bottle microresonator can be excited in both passive and lasing regimes by optical WGMs of this resonator [14]. The separation of optical WGM eigenfrequencies considered in [14] did not match acoustic eigenfrequencies, i.e., were not resonant. In this Letter, we introduce and study a bottle resonator with a nanoscale parabolic ERV (Fig. 1) which exhibits resonant interaction of optical and acoustic modes. We show that an acoustic mode localized in this resonator, which resonantly interacts with an optical WGM, can parametrically generate a series of optical modes with a highly equidistant spectrum forming a moderately broadband optical frequency comb (OFC).

We consider slow optical WGMs numerated by azimuthal, radial, and axial quantum numbers, m , n , and q , respectively. The slowness of modes is determined by the proximity of their eigenfrequency ν to a cutoff frequency ν_{cut} (see, for example, [13]). In contrast to spherical and toroidal microresonators [1–7,15,16], the separation of eigenfrequencies of a bottle resonator along the quantum number q can be made very small, without increasing the resonator cross-sectional radius r_0 (see, for example, [13]). This makes the bottle resonator very attractive for the investigation of interactions between its optical WGMs and acoustic modes. The acoustic modes of our interest are the axially symmetric breathe modes with zero azimuthal quantum number, $m_{\text{ac}} = 0$, illustrated in Fig. 1(a). These modes can be excited by the radiation pressure of an optical WGM whose magnitude is modulated with the frequency of the chosen acoustic mode. In turn, an axially symmetric acoustic

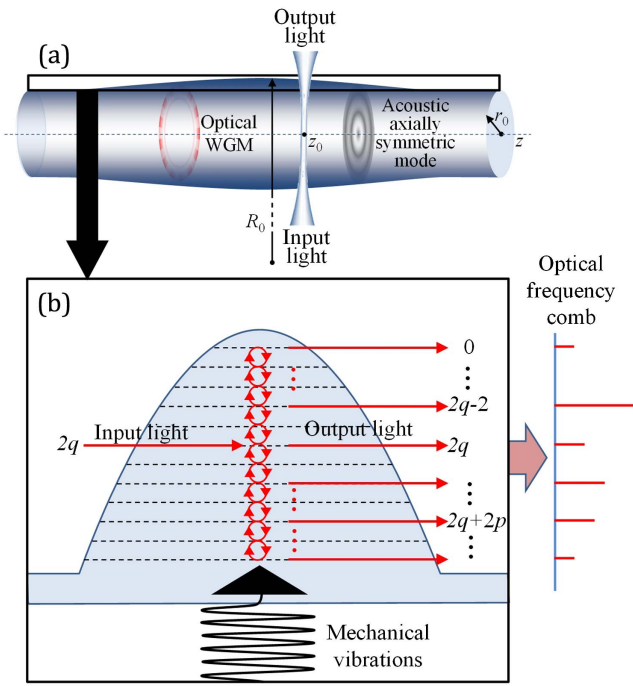


Fig. 1. (a) Illustration of a bottle microresonator holding an optical WGM and an acoustic axially symmetric mode. Light is coupled in and out of the resonator by a microfiber taper which is aligned normally to the resonator axis z . (b) Excitation of the optical modes with even axial quantum numbers by an acoustic mode which is symmetric with respect to axis z leading to the generation of an equidistant OFC.

mode with eigenfrequency $\nu^{(\text{ac})}$ causes resonant coupling of optical modes with the same m if the difference of their eigenfrequencies $\Delta\nu^{(\text{op})}$ along the quantum number q matches $\nu^{(\text{ac})}$. Crucially, the clamping losses of the considered acoustic modes can be eliminated, since the optical fiber hosting a bottle resonator can be clamped in the regions completely separated from the acoustic mode location.

Provided that the power of optical WGMs is relatively small so that the back-action effects [1] can be ignored, variation of a slow optical WGM along the bottle axis z is described by the Schrödinger equation [17]

$$\frac{i}{2\pi\nu_{\text{cut}}}\frac{\partial\Psi}{\partial t} + \frac{1}{2\beta_{\text{cut}}^2}\frac{\partial^2\Psi}{\partial z^2} + \frac{\Delta r(z,t)}{r_0}\Psi = A_{\text{in}}(z,t), \quad (1)$$

where $\beta_{\text{cut}} = 2\pi\nu_{\text{cut}}n_r/c$ is the cutoff wavenumber, n_r is the refractive index of the fiber material, c is the speed of light, and $\Delta r(z,t) = r(z,t) - r_0$ is the ERV of the fiber. The source term $A_{\text{in}}(z,t)$ in this equation generalizes the stationary expression for the input of light from the microfiber coupled to the bottle resonator at $z = z_0$ [Fig. 1(a)] [18] to the nonstationary case:

$$A_{\text{in}}(z,t,\nu) = A_0\delta(z-z_0)\exp(-2\pi i(\nu-\nu_{\text{cut}})t) \begin{cases} \exp(2\pi\gamma t) & t < 0 \\ 1 & t \geq 0 \end{cases}, \quad (2)$$

where $\delta(x)$ is the delta-function, ν is the frequency of the input light, and γ^{-1} characterizes the switching time, which is usually much greater than the lifetime of optical modes. The effect of

mechanical vibrations of our concern, whose amplitude is typically several of the ERV, has the negligible effect on the coupling between the microfiber and the resonator.

The excitation of the optical modes of a bottle resonator by its natural mechanical vibration with frequency $\nu^{(\text{ac})}$ is modeled by Eq. (1) with $\Delta r(z,t) = \Delta r(z) + \eta(z)\sin(2\pi\nu^{(\text{ac})}t)$, where $\Delta r(z)$ is the unperturbed nanoscale profile of the resonator and $\eta(z) \ll \Delta r(z)$ is the axial distribution of the amplitude of the excited acoustic mode. In the presence of acoustic oscillation with frequency $\nu^{(\text{ac})}$, the solutions of Eq. (1) can be expressed through Floquet quasi-states [19]:

$$\Psi_q(z,t) = \exp[-2\pi i(\zeta_q - \nu_{\text{cut}})t] \times \sum_{p=-\infty}^{\infty} \exp[-2\pi i(p \text{Re } \nu^{(\text{ac})} + |p| \text{Im } \nu^{(\text{ac})})t] U_{q,p}(z), \quad (3)$$

where ζ_q is a quasi-frequency, q is the axial quantum number, and quantum numbers m and n are omitted for brevity. In Eq. (3), $\text{Im } \nu^{(\text{ac})}$ characterizes the attenuation of mechanical oscillations so that the acoustic Q -factor is determined as $Q^{(\text{ac})} = \text{Re } \nu^{(\text{ac})} / \text{Im } \nu^{(\text{ac})}$. Due to the proximity of frequency $\nu^{(\text{ac})}$ and the spacing between optical eigenfrequencies $\Delta\nu^{(\text{op})}$, we assume that the transition amplitudes between quasi-states $\Psi_q(\mathbf{r},t)$ is much greater than the transition amplitudes between these quasi-states and other quasi-states of the resonator. Then, the expression for the non-stationary Green's function of the Schrödinger equation [20] will include only the series $\{\Psi_q(\mathbf{r},t)\}$ of our interest:

$$G(z_1, z_2, t_1, t_2) = \theta(t_1 - t_2) \sum_q \Psi_q(z_1, t_1) \Psi_q^*(z_2, t_2), \quad (4)$$

where $\theta(x)$ is the Heaviside step function.

The eigenfrequencies of a high Q -factor optical microresonator are usually detected by measuring the resonant transmission amplitude of light evanescently coupled to the resonator through a waveguide [Fig. 1(a)]. For weak coupling between the input-output waveguide and the resonator (strong under-coupled regime [16]), the inelastic output amplitude [corresponding to $|p_2| + |p_1| \neq 0$ in Eq. (5)] is found from Eqs. (2)–(4) as

$$A_{\text{out}}(\nu_1, \nu_2) = \int_{-\infty}^{\infty} dt_2 \int_{-\infty}^{t_2} dt_1 \int_{-\infty}^{\infty} dz_1 G(z_1, z_2, t_1, t_2) A_{\text{in}}(z_1, t_1, \nu_1) = A_0 \sum_{q,p_1,p_2} U_{q,p_1}(z_0) U_{q,p_2}^*(z_0) \times \{ (p_2 \text{Re } \nu^{(\text{ac})} - i|p_2| \text{Im } \nu^{(\text{ac})} + \zeta_q - \nu_1) \times [(p_1 - p_2) \text{Re } \nu^{(\text{ac})} - i(|p_1| + |p_2|) \text{Im } \nu^{(\text{ac})} + \nu_2 - \nu_1] \}^{-1}. \quad (5)$$

Consider the important case when the input optical frequency is equal to the bottle resonator eigenfrequency, $\nu_1 = \text{Re}(\zeta_q)$. Then, the equally spaced OFC teeth are determined from Eq. (5) as

$$\nu_2 = \text{Re}(\zeta_q) + p \text{Re } \nu^{(\text{ac})}, \quad p = \pm 1, \pm 2, \dots \quad (6)$$

Equation (6) shows that, in contrast to the frequency of mechanical vibrations generated by optomechanical back-action [1] and the repetition rate of the OFC generated due

to Kerr nonlinearity [21], the spacing between the teeth maxima in our case is fully determined by the natural acoustic frequency $\text{Re}\nu^{(\text{ac})}$. Provided that the heating effects are small, this frequency does not depend on the input optical power and mechanical vibration amplitude. The power of the generated OFC teeth is determined from Eq. (5) as

$$\Omega_{q,p} = \frac{|A_0 U_{q,0}(z_0) U_{q,p}^*(z_0)|^2}{(\text{Re}\nu^{(\text{ac})} \text{Re}\zeta_q)^2 p^2} (Q^{(\text{opt})} Q^{(\text{ac})})^2. \quad (7)$$

From this equation, the power of the teeth is proportional to the squared product of the optical Q -factor, $Q^{(\text{opt})} = \text{Re}\zeta_q / \text{Im}\zeta_q$, and acoustic Q -factor, $Q^{(\text{ac})} = \text{Re}\nu^{(\text{ac})} / \text{Im}\nu^{(\text{ac})}$.

To illustrate the general results described by Eqs. (5)–(7), we consider the parametric excitation of optical modes in a parabolic bottle resonator perturbed by the axially symmetric acoustic mode with $m_{\text{ac}} = 0$, $n_{\text{ac}} = 1$, and $q_{\text{ac}} = 0$. We simplify the problem by approximating the Gaussian axial distribution of the amplitude of this mode by a parabola. Then,

$$\Delta r(z, t) = -\frac{z^2}{2R_0} (1 + 2\varepsilon \sin(2\pi\nu^{(\text{ac})}t)), \quad \varepsilon \ll 1. \quad (8)$$

In addition, we assume that the input of light is situated in the middle of the resonator [$z_0 = 0$ in Eq. (2) and Fig. 1(a)]. In this case, the excited optical and acoustic modes have the same reflection symmetry ($\Psi(z, t) = \Psi(-z, t)$), and mechanically generated transitions will only exist between the WGMs with axial quantum numbers q of even parity. Parametric excitation of these modes takes place for acoustic oscillations with a frequency close to $2\Delta\nu^{(\text{op})} = 2c(2\pi n_r)^{-1}(-r_0 R_0)^{-1/2}$:

$$\nu^{(\text{ac})} = \Delta\nu^{(\text{op})} (2 + \delta), \quad \delta \ll 1, \quad (9)$$

which is twice as large as that for a general asymmetric case considered above. While the model of the vibrating parabolic resonator described by Eq. (8) cannot fit the axial distribution of an acoustic mode exactly, it is remarkably accurate for relatively small quantum numbers q of optical modes. As an example, Fig. 2(a) shows the nanoscale ERV of a silica bottle resonator with $r_0 = 20 \mu\text{m}$ for the acoustic mode with quantum numbers $m_{\text{ac}} = 0$, $n_{\text{ac}} = 1$, and $q_{\text{ac}} = 0$ corresponding to $R_0 = 3.3 \text{ km}$ and $\nu^{(\text{ac})} = 2\Delta\nu^{(\text{op})} = 255 \text{ MHz}$ calculated using theory [13]. Figure 2(b) compares the axial distribution of this acoustic mode with a parabola. A comparison of this distribution with those of optical WGMs with $q = 0, 10$ and 50 in Fig. 2(c) shows that the parabolic approximation of Eq. (8) is justified for axial quantum numbers q of several tens. The number of axial modes situated in the fiber segment with nanoscale ERV $\Delta r_0 \sim 2 \text{ nm}$ and length $\sim 5 \text{ mm}$ [Fig. 2(a)] is estimated as $\nu_0^{(\text{op})} \Delta r_0 / (\Delta\nu^{(\text{op})} r_0) \sim 200$.

Equation (1) with the ERV defined by Eq. (8) can be solved analytically [22]. Under the conditions of Eqs. (8) and (9), i.e., $\varepsilon \ll 1$, $\delta \ll 1$, we find that the parametrically generated frequency combs are defined by Eqs. (5)–(7), where $z_0 = 0$, $U_{2q+1,p}(0) = 0$, and

$$U_{2q,p}(0) = \frac{[(2q)!]^{1/2}}{(-2)^q q!} \left(\frac{\pi f \kappa}{\pi(1+\kappa)} \right)^{1/2} \sum_{n=\max(0,p)}^{2q} \binom{2q}{n} \binom{-2q-1/2}{n-p} \left(\frac{1-\kappa}{1+\kappa} \right)^{2n-p},$$

$$\kappa = \left(1 - \frac{\varepsilon}{\delta} \right)^{1/2} \left(1 + \frac{\varepsilon}{\delta} \right)^{-1/2}. \quad (10)$$

From this equation, the inelastic transmission amplitude, Eq. (5), and comb teeth power, Eq. (7), depend only on the ratio of relative amplitude of vibrations and relative deviation

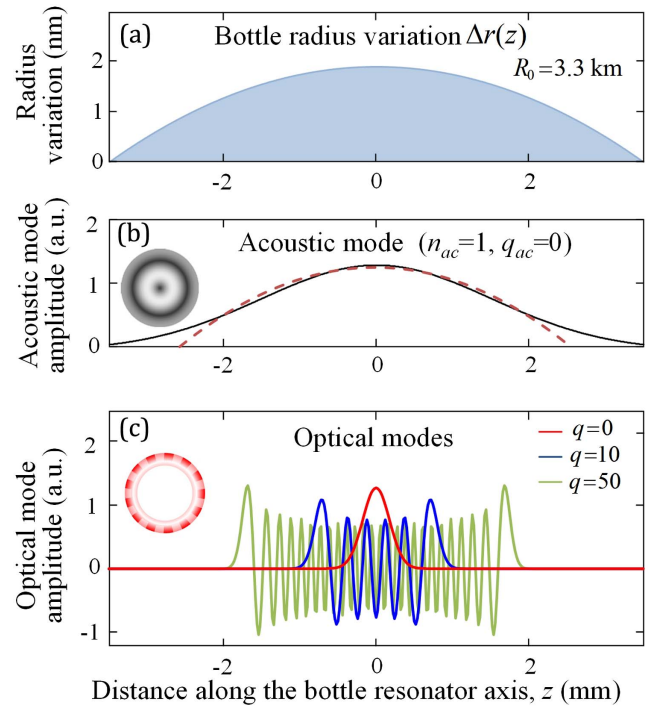


Fig. 2. Comparison of optical and acoustic mode distributions for a bottle resonator having the eigenfrequency $\nu^{(\text{ac})}$ of an acoustic mode equal to the spacing of optical eigenfrequencies $\Delta\nu^{(\text{op})}$ along the quantum number q . (a) Nanoscale ERV of this resonator. (b) Axial distribution of the acoustic mode with quantum numbers $m_{\text{ac}} = 0$, $n_{\text{ac}} = 1$, and $q_{\text{ac}} = 0$ fitted by a parabola (dashed curve). (c) Axial distribution of optical modes with $q = 0$, $q = 10$, and $q = 50$.

of acoustic eigenfrequency from the optical eigenfrequency spacing, ε/δ , which formally can be arbitrarily small. Figure 3 shows the power of the frequency comb teeth for $\varepsilon/\delta = 0.1, 0.3, 0.5$, and 0.9 and constant $\text{Im}\zeta_q$. It is seen that the bandwidth of combs grows with ε/δ and can be significant when this ratio approaches unity [19]. At the same time, it follows from Eq. (10) that the power of the teeth slowly vanishes as $\varepsilon/\delta \rightarrow 1$. The plots in Fig. 3 also show that the behavior of comb tooth heights $\Omega_{2q,p}$ is irregular as a function of quantum numbers q and p . This is analogous to the behavior of transition probabilities in a quantum mechanical time-dependent harmonic oscillator described by the same Schrödinger equation [18]. The increase of asymmetry of the graphs with growing ε/δ is explained by approaching the ground states at $2q + p = 0$.

Note that the acoustic eigenfrequency $\nu^{(\text{ac})}$ of the bottle resonator is surrounded by adjacent eigenfrequencies of acoustic modes with non-zero axial quantum numbers q_a [9]. The separation of these eigenfrequencies, $\Delta\nu^{(\text{ac})}$, is usually much smaller than the width $\text{Im}\zeta_q$ of optical eigenfrequencies. At room temperature, this separation is also smaller than the width of acoustic eigenfrequencies, $\Delta\nu^{(\text{ac})} < \text{Im}\nu^{(\text{ac})}$. The opposite condition $\Delta\nu^{(\text{ac})} \gg \text{Im}\nu^{(\text{ac})}$, which corresponds to very high mechanical Q -factors $Q_{\text{mech}} > 10^5$, can be achieved at very low temperatures below $T \sim 0.1 \text{ K}$ [24,25]. The elimination of acoustic modes with large q_{ac} can be performed by clamping the bottle resonator in the region where these modes are situated [Fig. 2(c)].

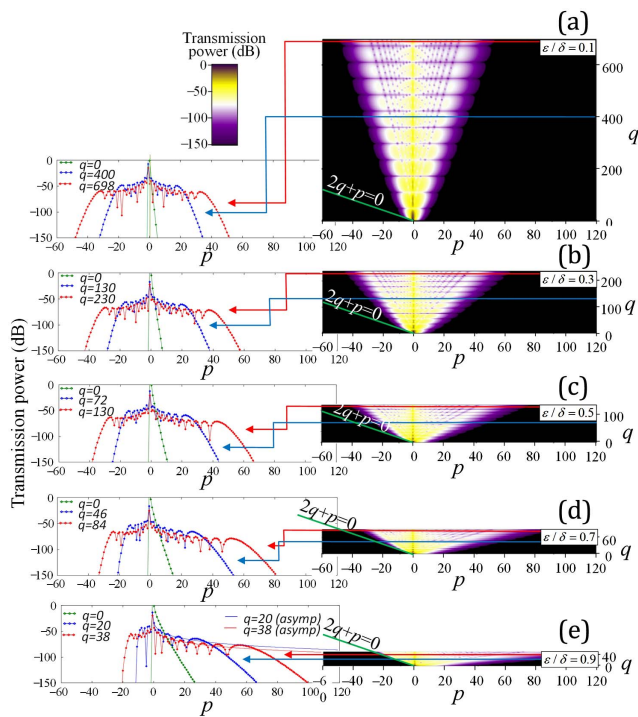


Fig. 3. Surface plots of the power of a generated OFCs as a function of quantum numbers p and q and graphs of these dependencies for fixed quantum numbers q . (a) $\epsilon/\delta = 0.1$, (b) $\epsilon/\delta = 0.3$, (c) $\epsilon/\delta = 0.5$, (d) $\epsilon/\delta = 0.7$, and (e) $\epsilon/\delta = 0.9$. The green lines defined by equation $2q + p = 0$ indicate the axial ground state of the bottle resonator.

In summary, it is shown that an OFC can be generated in an optical bottle microresonator with an equidistant spectrum by its natural mechanical vibrations. In practice, small deviations from the spectral equidistance are introduced by fabrication errors. However, these deviations affect the OFC teeth power, rather than their equidistance, which is defined by the natural frequency of vibrations $\nu^{(ac)}$. Generally, the power of OFCs generated mechanically is inverse proportional to the squared product of their optical and mechanical Q -factors. Provided that these Q -factors are large enough, the power required for the generation of these combs can be remarkably small and only limited by the sensitivity of the optical detectors.

Funding. Royal Society (WM130110); Horizon 2020 Framework Programme (H2020) (H2020-EU.1.3.3, 691011); Engineering and Physical Sciences Research Council (EPSRC) (EP/P006183/1).

Acknowledgment. The author acknowledges the Royal Society Wolfson Research Merit Award.

REFERENCES AND NOTES

1. M. Aspelmeyer, T. J. Kippenberg, and F. Marquardt, *Rev. Mod. Phys.* **86**, 1391 (2014).
2. A. B. Matsko, A. A. Savchenkov, V. S. Ilchenko, D. Seidel, and L. Maleki, *Phys. Rev. Lett.* **103**, 257403 (2009).
3. A. A. Savchenkov, A. B. Matsko, V. S. Ilchenko, D. Seidel, and L. Maleki, *Opt. Lett.* **36**, 3338 (2011).
4. G. Bahl, J. Zehnpfennig, M. Tomes, and T. Carmon, *Nat. Commun.* **2**, 403 (2011).
5. I. S. Grudinin, H. Lee, O. Painter, and K. J. Vahala, *Phys. Rev. Lett.* **104**, 083901 (2010).
6. I. S. Grudinin, A. B. Matsko, and L. Maleki, *Phys. Rev. Lett.* **102**, 043902 (2009).
7. H. Lee, T. Chen, J. Li, K. Y. Yang, S. Jeon, O. Painter, and K. J. Vahala, *Nat. Photonics* **6**, 369 (2012).
8. M. Asano, Y. Takeuchi, S. K. Ozdemir, R. Ikuta, L. Yang, N. Imoto, and T. Yamamoto, *Opt. Express* **24**, 12082 (2016).
9. T. Tetsumoto and T. Tanabe, *ALP Adv.* **4**, 077137 (2014).
10. M. Sumetsky, *Nanophotonics* **2**, 393 (2013).
11. M. Sumetsky, *Phys. Rev. Lett.* **111**, 163901 (2013).
12. N. A. Toropov and M. Sumetsky, *Opt. Lett.* **41**, 2278 (2016).
13. M. Sumetsky, *Opt. Lett.* **42**, 923 (2017).
14. M. Asano, Y. Takeuchi, W. Chen, Ş. K. Özdemir, R. Ikuta, N. Imoto, L. Yang, and T. Yamamoto, *Laser Photonics Rev.* **10**, 603 (2016).
15. K. Vahala, *Nature* **424**, 839 (2003).
16. A. B. Matsko and V. S. Ilchenko, *IEEE J. Quantum Electron.* **12**, 3 (2006).
17. M. Sumetsky, *Sci. Rep.* **5**, 18569 (2015).
18. M. Sumetsky, *Opt. Express* **20**, 22537 (2012).
19. S. Kohler, J. Lehmann, and P. Hänggi, *Phys. Rep.* **406**, 379 (2005).
20. J. D. Bjorken and S. D. Drell, *Relativistic Quantum Mechanics* (McGraw-Hill, 1964).
21. T. J. Kippenberg, R. Holzwarth, and S. A. Diddams, *Science* **332**, 555 (2011).
22. A. M. Perelomov and Y. B. Zel'dovich, *Quantum Mechanics: Selected Topics* (World Scientific, 1998).
23. Notice that the absence of sharp elastic transmission peaks at $p = 0$ in the plots of Fig. 3 is due to the fact that the major elastic component of the transmission amplitude has been omitted in Eq. (10).
24. R. O. Pohl, X. Liu, and E. Thompson, *Rev. Mod. Phys.* **74**, 991 (2002).
25. A. D. Fefferman, R. O. Pohl, A. T. Zehnder, and J. M. Parpia, *Phys. Rev. Lett.* **100**, 195501 (2008).